Journal of Medicinal Chemistry

Article

pubs.acs.org/jmc

Discovery and Optimization of a Series of 2-Aryl-4-Amino-5-(3′,4′,5′-trimethoxybenzoyl)Thiazoles as Novel Anticancer Agents

Romeo Romagnoli,*[,†] Pier Giovanni Baraldi,*[,†] Maria Kimatrai Salvador,[†] Delia Preti,[†] Mojgan Aghazadeh Tabrizi,[†] Andrea Brancale,[‡] Xian-Hua Fu,[§] Jun Li,[§] Su-Zhan Zhang,[§] Ernest Hamel,[∥] Roberta Bortolozzi,[⊥] Elena Porcù,[⊥] Giuseppe Basso,[⊥] and Giampietro Viola*[,⊥]

[†]Dipartimento di Scienze Chimiche e Farmaceutiche, Università di Ferrara, 44121 Ferrara, Italy

[‡]School of Pharmacy and Pharmaceutical Sciences, Cardiff University, King Edward VII Avenue, Cardiff CF10 3NB, U.K.

[§]Cancer Institute, Key Laboratory of Cancer Prevention and Intervention, China National Ministry of Education, The Second Affiliated Hospital, School of Medicine, Zhejiang University, Hangzhou, Zhejiang Province 310009, People's Republic of China

[∥]Screening Technologies Branch, Developmental Therapeutics Program, Division of Cancer Treatment and Diagnosis, Frederick National Laboratory for Cancer Research, National Cancer Institute, National Institutes of Health, Frederick, Maryland 21702, United States

[⊥]Dipartimento di Salute della Donna e del Bambino, Laboratorio di Oncoematologia, Università di Padova, 35131 Padova, Italy

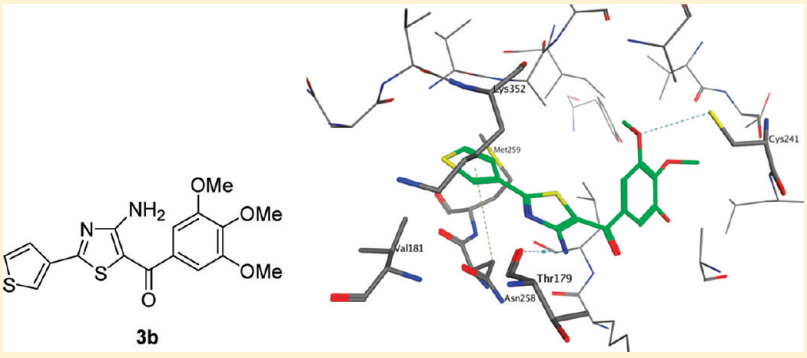

ABSTRACT: A new series of tubulin polymerization inhibitors based on the 2-aryl/heteroaryl-4-amino-5-(3′,4′,5′-trimethoxybenzoyl)thiazole scaffold was synthesized and evaluated for growth inhibition activity on a panel of cancer cell lines, cell cycle effects, and *in vivo* potency. Structure−activity relationships were elucidated with various substitutions at the 2-position of the thiazole skeleton. Hydrophobic moieties, such as phenyl and 3-thienyl, were well tolerated at this position, and variation of the phenyl substituents had remarkable effects on potency. The most active compound (**3b**) induced apoptosis through the mitochondrial pathway with activation of caspase-3. We also showed that it has potential antivascular activity since it reduced *in vitro* endothelial cell migration and disrupted capillary-like tube formation at noncytotoxic concentrations. Furthermore, compound **3b** significantly reduced the growth of the HT-29 xenograft in a nude mouse model, suggesting that **3b** is a promising new antimitotic agent with clinical potential.

INTRODUCTION

Besides being critical for cell architecture, the microtubule system of eukaryotic cells is essential for cell division since microtubules are key components of the mitotic spindle.[1] Microtubules are a dynamic cellular compartment in both neoplastic and normal cells. This dynamicity is characterized by the continuous turnover of $\alpha\beta$-tubulin heterodimers in the polymeric microtubules. The microtubule system is also important in other fundamental cellular processes, such as regulation of motility, cell signaling, formation and maintenance of cell shape, secretion, and intracellular transport.[2]

In the last decades, there has been a continuing interest in the discovery and development of novel small molecules able to inhibit tubulin polymerization.[3] Numerous chemically diverse antimitotic agents, many of which are natural products, interact specifically with tubulin.[4] Among the naturally occurring derivatives, combretastatin A-4 (CA-4, **1**, Chart 1), isolated from the bark of the South African tree *Combretum caffrum*,[5] is one of the well-known tubulin-binding molecules affecting microtubule dynamics, and compound **1** strongly inhibits the polymerization of tubulin by binding to the colchicine site.[6] Compound **1** shows potent cytotoxicity against a wide variety of human cancer cells, including those that are multidrug resistant.[7]

Received: March 21, 2012
Published: May 14, 2012

Chart 1. Chemical Structures of CA-4 and 2-Substituted-4-amino-5-aroylthiazoles 2a and 3a–o

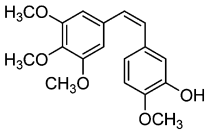

Combretastatin A-4 (CA-4), **1**

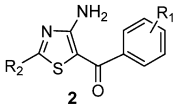

2

R_1=one, two or three OMe, H, halogen
R_2=NH_2, $N(CH_3)_2$, $N(C_2H_5)_2$,
pyrrolidin-1-yl, morpholin-4-yl, piperidin-1-yl

2a, R_1=3′,4′,5′-$(OCH_3)_3$, R_2=pyrrolidin-1-yl

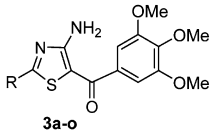

3a-o

3a, R=C_6H_5
3b, R=3-thienyl
3c, R=p-F-C_6H_4
3d, R=p-Cl-C_6H_4
3e, R=m-Cl-C_6H_4
3f, R=p-CH_3-C_6H_4
3g, R=p-C_2H_5-C_6H_4
3h, R=p-$C(CH_3)_3$-C_6H_4
3i, R=p-CF_3-C_6H_4
3j, R=p-OCH_3-C_6H_4
3k, R=m-OCH_3-C_6H_4
3l, R=m,p-$(OCH_3)_2$-C_6H_3
3m, R=p-OCH_2CH_3-C_6H_4
3n, R=p-OCF_3-C_6H_4
3o, R=p-NO_2-C_6H_4

In the course of our search for new synthetic tubulin inhibitors, we recently reported the synthesis and biological characterization of a series of 2-alkylamino-4-amino-5-aroylthiazoles with general structure **2**, prepared by an easy one-pot four step procedure.[8] Among the synthesized compounds, the 2-(pyrrolidin-1-yl)-4-amino-5-(3′,4′,5′-trimethoxybenzoyl)-thiazole derivative **2a** was the only compound of this series active at submicromolar concentrations against a panel of five cancer cell lines, with IC_{50} values ranging from 0.2 to 0.4 μM. Compound **2a** was 10- to 100-fold less active than the reference compound **1** as an antiproliferative agent, while it was comparable to **1** as an inhibitor of tubulin polymerization. Structure–activity relationship studies indicated that the pyrrolidine is the only substituent tolerated at the 2-position of the thiazole scaffold. This finding led us to assume that the tubulin binding pocket for this portion of the molecule is quite small and that tubulin only tolerated the presence of hydrophobic substituents, indicating the possibility for further improvement in activity. Thus, once the 4-amino-5-(3′,4′,5′-trimethoxybenzoyl) thiazole scaffold was identified as the minimum structural requirement for activity in this new series of compounds, our strategy for further development of active antimitotic agents was to perform modifications at the 2-position of the thiazole ring. The first round of optimization included replacement of the pyrrolidine ring of compound **2a** with a phenyl or bioisosteric 3-thienyl ring, to furnish derivatives **3a** and **3b**, respectively. As shown in Table 1, phenyl or 3′-thienyl substitutions at the C-2 position of the thiazole ring significantly enhanced antiproliferative activity. Encouraged by the increased potency obtained with **3a**, we then synthesized compounds **3c–o** to determine whether various electron-releasing (Me, Et, $C(CH_3)_3$, OMe, OEt, and OCF_3) or electron-withdrawing (F, Cl, CF_3, CN, and NO_2) substituents on the *para*- or *meta*-positions of the phenyl ring would further enhance activity. To compare the effects of *para*- and *meta*-substitution, the chloro atom and the methoxy-group were also introduced at the *meta*-position of the phenyl ring. We are including **3b** in this article because it had the best antiproliferative activity (see below) of all the compounds prepared in this study.

We examined the efficacy of the newly synthesized compounds on a panel of human cancer cell lines, including multidrug resistant lines overexpressing the 170-kDa P-glycoprotein drug efflux pump, and we investigated in detail the modalities of cell death induced by these derivatives. Since many antimitotic drugs, such as compound **1**, have been shown to possess anti-angiogenic and antivascular activities,[9,10] we also investigated the effects of these compounds on *in vitro* assays with HUVECs.

CHEMISTRY

The general synthesis of 2-aryl/heteroaryl-4-amino-5-(3′,4′,5′-trimethoxybenzoyl)thiazoles **3a–o** is outlined in Scheme 1. These molecules were prepared by a one-step efficient synthetic procedure, starting from an easily accessible common

Table 1. *In Vitro* Cell Growth Inhibitory Effects of Compounds 1 and 3a–o

	IC_{50}[a] (nM)					
compd	HeLa	A549	HL-60	Jurkat	MCF-7	HT-29
3a	7.6 ± 1.7	367 ± 11.0	80.8 ± 7.1	58.0 ± 5.6	2.2 ± 0.8	13.2 ± 5.4
3b	2.4 ± 0.9	210 ± 38.1	77.9 ± 2.6	26.4 ± 2.3	51.2 ± 9.3	11.4 ± 2.8
3c	24.1 ± 4.3	1082 ± 36.7	384 ± 25.0	582 ± 15.4	29.4 ± 1.5	115 ± 3.5
3d	188 ± 46.0	6730 ± 202	4445 ± 68.2	1749 ± 58.8	845 ± 18.5	2083 ± 50.5
3e	2.8 ± 1.0	326 ± 14.8	137 ± 27.2	35.9 ± 4.4	41.7 ± 3.5	24.0 ± 5.8
3f	22.7 ± 7.8	1223 ± 97.1	295 ± 27.0	201 ± 57.1	3.2 ± 0.7	53.1 ± 14.8
3g	191 ± 44.8	5175 ± 135	1813 ± 244	2328 ± 577	1583 ± 267	1018 ± 135
3h	4148 ± 75.4	>10,000	>10,000	>10,000	508 ± 123	9067 ± 158
3i	1799 ± 27.6	>10,000	>10,000	>10,000	>10,000	>10,000
3j	244 ± 41.3	>10,000	>10,000	2023 ± 75.9	1255 ± 25.7	2806 ± 72.2
3k	13.7 ± 4.5	720 ± 28.3	41.2 ± 5.5	66.6 ± 8.9	11.3 ± 5.1	22.3 ± 4.4
3l	191 ± 35.9	>10,000	1136 ± 74.4	606 ± 45.7	257 ± 65.4	220 ± 18.6
3m	1981 ± 36.0	6253 ± 318	>10,000	4829 ± 64.1	>10,000	>10,000
3n	>10,000	>10,000	>10,000	>10,000	>10,000	>10,000
3o	570 ± 10.2	6106 ± 169.9	>10,000	>10,000	>10,000	4785 ± 83.2
1	4 ± 1	180 ± 50	1 ± 0.2	5 ± 0.6	370 ± 100	3100 ± 100

[a]IC_{50} = compound concentration required to inhibit tumor cell proliferation by 50%. Data are expressed as the mean ± SEM from the dose–response curves of at least three independent experiments.

dx.doi.org/10.1021/jm300388h | *J. Med. Chem.* 2012, 55, 5433–5445

Scheme 1[a]

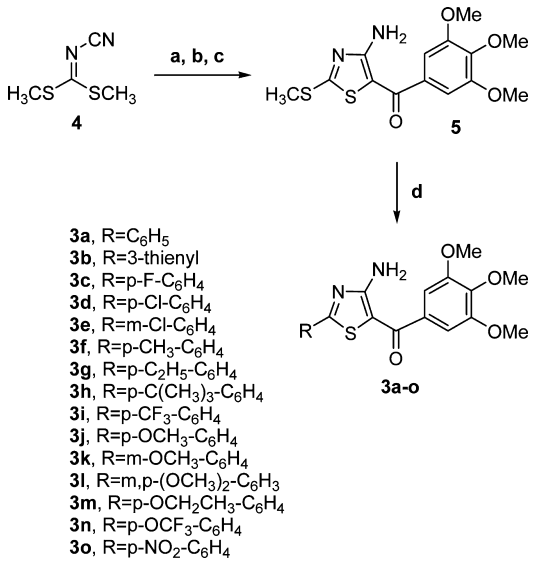

[a]Reagents: a, $Na_2S{\cdot}9H_2O$, DMF, 70 °C, 2 h; b, 1-(3′,4′,5′-trimethoxyphenyl)-2-bromoethanone, 50 °C, 2 h; c, K_2CO_3, 1 h; d, Pd_2dba_3, Cu(I)Tc, TFP, $ArB(OH)_2$, THF, 60 °C, 18 h.

intermediate **5**.[8] This latter compound was obtained in good yield by a one-pot three-step sequential procedure, starting from dimethyl cyanodithiocarbonate **4**, which was reacted successively with sodium sulfide, 2-bromo-1-(3,4,5-trimethoxyphenyl)ethanone and potassium carbonate.[11] The Pd_2dba_3-catalyzed, Cu(I)Tc-mediated coupling of thiazole-2-thiomethyl ether **5** with the appropriate aryl/heteroaryl boronic acid, in the presence of TFP, furnished the 2-aryl/heteroaryl substituted thiazoles **3a**–**o** in high yields, avoiding the protection/deprotection sequence of the amino group at the 4-position of the thiazole ring.[12]

BIOLOGICAL RESULTS AND DISCUSSION

***In Vitro* Antiproliferative Activities.** The 2-aryl/heteroaryl-4-amino-5-(3′,4′,5′-trimethoxybenzoyl)thiazoles **3a**–**o** were evaluated for their antiproliferative activity against a panel of six human tumor cell lines and compared with reference compound **1**. As shown in Table 1, the antiproliferative activities of the tested compounds were generally more pronounced against HeLa and MCF-7 cells as compared with the other cell lines. With the exception of MCF-7 cells, the 3-thienyl derivative **3b** was the most active compound in this series, exhibiting IC_{50} values ranging from 2.4 to 78 nM against five of the six cancer cell lines and an IC_{50} of 210 nM against the A549 cells. Moreover, with the MCF-7 and HT-29 cells, compounds **3a**–**c**, **3e**–**f**, and **3k** were more potent than **1**, with IC_{50} values in the single- or double-digit nanomolar range. Compounds **3b** and **3e** showed comparable potency to **1** against the HeLa cells. Of the 15 tested compounds, **3a**–**b**, **3e**, and **3k** possessed the highest overall potency, with IC_{50} values of 2.4–140 nM against five of the six cancer cell lines and IC_{50} values of 200–700 nM against the A549 cells. With the exception of MCF-7 and HT-29 cells, reference compound **1** possessed the highest potency in four of the six cell lines tested.

The bioisosteric replacement of the phenyl ring of compound **3a** with the 3-thienyl group (**3b**) produced a 1.5- to 3-fold increase of potency against A549, Jurkat, and HeLa cells, while the differences between **3a** and **3b** were minimal in HL-60 and HT-29 cells. Only in MCF-7 cells was **3b** less active than **3a** (IC_{50} values of 51 and 2.2 nM, respectively). Excluding the A549 cells, compounds **3a** and **3b** had IC_{50} values ranging from 24 to 80 nM against the cell lines, compared with a range of 1–3100 nM obtained with **1**.

The data shown in Table 1 demonstrated the importance of substituents on the phenyl ring at the 2-position of the thiazole system for activity and selectivity against the different cancer cell lines. In general, all substituents caused a reduction in antiproliferative activity relative to **3a**, except in four cases. The *meta*-chloro substituent of **3e** resulted in enhanced antiproliferative activity against three cell lines (HeLa, A549, and Jurkat cells), while the *meta*-methoxy substituent of **3k** resulted in enhanced activity in one cell line (HL-60 cells). Otherwise, all substituents led to reduced activity, sometimes mild to moderate (e.g., **3c**, **3e**, and **3f**) and sometimes profound (e.g., **3h**–**j** and **3l**–**o**).

Turning specifically to the *para*-substituted phenyl derivatives, these showed highly variable potencies. Generally, it was found that most substituents in the *para*-position resulted in lower activity as compared to the unsubstituted parent compound **3a**, with the least deleterious being fluorine and methyl (compounds **3c** and **3f**, respectively). Comparing the fluorine derivative (**3c**) with the methyl derivative (**3f**), the latter was more active in five of the six cell lines we examined, with the greatest difference observed in the MCF-7 cells. Comparing the fluorine (**3c**) and the chlorine (**3d**) derivatives, increasing the size of the halide led to a large loss of activity with all six cell lines. In contrast, as noted above, the *meta*-chloro derivative (**3e**) was much more active than its *para*-congener **3d**, including enhanced activity relative to **3a** in three cell lines. Indeed, the activity of **3e** did not differ greatly from the 3-thienyl analogue **3b** in all cell lines.

Turning to the electronic characteristics of the *para*-substituents, the introduction of a weak electron-releasing methyl group (**3f**) caused a 1.5–4-fold loss in antiproliferative activity in the six cell lines relative to the unsubstituted **3a**. A *para*-ethyl group (compound **3g**) caused a further, major decrease in antiproliferative activity relative to **3a**, and **3f** was 14–700-fold less active in the six cell lines. Little antiproliferative activity was observed with still larger *para*-substituents (**3h**–**j**, **3m**–**o**), regardless of their electronic characteristics.

The antiproliferative activities of compounds **3j**, **3k**, and **3l** were influenced by the number and position of methoxy substituents on the phenyl ring. The *meta*-methoxy derivative **3k**, as noted above, was relatively active. Relative to the unsubstituted **3a**, **3k** was 1.1–5-fold less active in five cell lines and twice as active in HL-60 cells. In contrast, the *para*-methoxy derivative **3j** was 32–570-fold less active than **3a** when IC_{50} values could be determined. The 3,4-dimethoxy substituted analogue **3l** was generally intermediate in activity between **3j** and **3k**.

In summary, comparing the effects of ERGs and EWGs on the phenyl at the C2-thiazole position, no consistent difference in effects on antiproliferative activity occurred. Overall, all substituents at the *para*-position led to a loss of activity, and profound loss occurred with larger substituents. The effects of the two small *meta*-substitents examined were not dramatic, leading, perhaps, to some enhancement of antiproliferative activity. In different cell lines, moreover, different effects were observed. For example, replacement of the electron-donating methoxy group with the electron-withdrawing chlorine atom (compounds **3k** and **3e**, respectively), resulted in a 3- and

dx.doi.org/10.1021/jm300388h | J. Med. Chem. 2012, 55, 5433–5445

4-fold reduction in activity against HL-60 and MCF-7 cells, while **3k** and **3e** showed comparable potencies against HT-29, and **3e** was 5- and 2-fold more active than **3k** against HeLa and Jurkat cells.

Effect of Compound 3b on Multidrug Resistant Cells. To investigate whether these derivatives are substrates of drug efflux pumps, one of the most active compounds (**3b**) was tested against a panel of drug resistant cell lines which either overexpress P-glycoprotein ($Lovo^{Doxo}$ and Cem^{Vbl100})[13,14] or are associated with tubulin gene mutations (A549-T12)[15] that result in modified tubulin with impaired polymerization properties. As shown in Table 2, **3b** exhibited cytotoxic activity

Table 2. *In Vitro* Cell Growth Inhibitory Effects of Compound 3b on Drug Resistant Cell Lines

	IC_{50}[a] (nM)		
compd	LoVo	$LoVo^{Doxo}$	resistance ratio[b]
3b	18.0 ± 4.5	24.8 ± 5.3	1.4
doxorubicin[c]	120 ± 30	13150 ± 210	109.6
	CEM	CEM^{Vbl100}	resistance ratio[b]
3b	273.3 ± 20.3	666.7 ± 12.0	2.4
vinblastine	0.8 ± 0.1	205 ± 46	256.2
	A549	A549-T12	resistance ratio[b]
3b	209.6 ± 38.1	201.5 ± 46.7	0.96
taxol[c]	7.2 ± 0.1	75.2 ± 12.5	10.4

[a]IC_{50}= compound concentration required to inhibit tumor cell proliferation by 50%. Data are expressed as the mean ± SEM from the dose−response curves of at least three independent experiments. [b]The values express the ratio between IC_{50} determined in resistant and nonresistant cell lines. [c]Data are from ref 8.

in all three of the drug resistant cell lines. The activity in the two P-glycopprotein overexpressing cell lines demonstrated that **3b** is not a substrate for this important drug pump.

Inhibition of Tubulin Polymerization and Colchicine Binding. To investigate whether the antiproliferative activities of compounds **3a−c**, **3e−f**, and **3k** derived from an interaction with tubulin, these agents were evaluated for their inhibition of tubulin polymerization and for effects on the binding of [^{3}H]colchicine to tubulin (Table 3).[16a,b] For comparison,

Table 3. Inhibition of Tubulin Polymerization and Colchicine Binding by Compounds 1, 3a−c, 3e−f and 3k

compd	tubulin assembly[a] IC_{50} ± SD (μM)	colchicine binding[b] % ± SD
3a	1.6 ± 0.2	78 ± 6
3b	1.5 ± 0.2	77 ± 4
3c	2.7 ± 0.2	45 ± 6
3e	1.7 ± 0.2	63 ± 3
3f	1.5 ± 0.1	59 ± 4
3k	2.2 ± 0.3	51 ± 6
1	1.2 ± 0.1	98 ± 0.6

[a]Inhibition of tubulin polymerization. Tubulin was at 10 μM. [b]Inhibition of [^{3}H]colchicine binding. Tubulin, colchicine, and the tested compound were at 1, 5, and 5 μM, respectively.

compound **1** was examined in contemporaneous experiments. In the assembly assay, compounds **3a−b** and **3e−f** were found to be the most active compounds (IC_{50} values, 1.5−1.7 μM), with activity comparable with that of **1** (IC_{50}, 1.2 μM). Compounds **3c** and **3k** were half as active as **1**, although they were more potent than **1** as antiproliferative agents against MCF-7 and HT-29 cells.

When comparing the inhibition of tubulin polymerization versus the growth inhibitory effects, we found a positive correlation for most, but not all, of the active compounds. While **3f** was generally less potent than **3b** as an antiproliferative agent, **3f** and **3b** showed equal potency as inhibitors of tubulin assembly. Similarly, **3k** is 1.5-fold less active than **3f** in the tubulin assay, but **3k** is more active than **3f** in five of the cell lines. Such discrepancies in antitubulin versus antiproliferative activity are not infrequently observed, but the reasons are usually uncertain, as in our case. Among possible explanations is that we used bovine brain tubulin in the former studies, and its composition in terms of tubulin isotypes differs significantly from that of different human cancer cell lines.[16c]

In the colchicine binding studies, derivatives **3a** and **3b** potently inhibited the binding of [^{3}H]colchicine to tubulin, with 79% and 77% inhibition occurring with these agents. Inhibition of colchicine binding by compounds **3c**, **3e−f**, and **3j** was lower, ranging from 45 to 63%. None, however, was quite as potent as **1**, which in these experiments inhibited colchicine binding by 98%.

For the most active compounds **3a** and **3b**, a good correlation was observed between antiproliferative activities, inhibition of tubulin polymerization, and inhibition of colchicine binding. In general, inhibition of [^{3}H]colchicine binding to tubulin correlated more closely with antiproliferative activity than did inhibition of tubulin assembly.

Molecular Modeling. A series of molecular docking simulations were performed to rationalize the observed SARs for this series of compounds. The proposed binding mode that emerged from these studies is virtually identical to the pyrrolidine analogue **2a** reported previously.[8] Figure 1 shows how the thienyl analogue **3b** sits in a tight hydrophobic pocket defined by β-tubulin residues Val181, Asn258, Met259, and Lys352. It is interesting to note that this pocket can only accommodate an aromatic ring with relatively small substituents, like the ones present in **3a**, **3c−f**, and **3k** (Figure 2), while compounds with bulkier substituents (e.g., the *t*-butyl of **3h**) do not dock well in the binding site because of steric hindrance. In addition to these nonpolar interactions, the trimethoxyphenyl ring of **3b** is also in contact with βCys241, while the amino group establishes a hydrogen bond with βThr179. These latter two interactions are often observed in models of the binding of tubulin inhibitors in the colchicine site.[17]

Analysis of Cell Cycle Effects. The effect of **3a** and **3b** on cell cycle progression was examined by flow cytometry in HeLa and Jurkat cells. Treatment with the two compounds in HeLa cells, resulted in the accumulation of cells in the G2/M phase, with a concomitant reduction in cells in both the S and G1 phases. These changes occurred in a concentration-dependent manner (Figure 3, panel A), but changes were observed even at the lowest concentration (62 nM) used. A similar behavior was observed also for Jurkat cells (Figure 3, panel B), except that for compound **3a** we detected a less pronounced G2/M arrest in comparison with **3b** in the same cell lines accompanied with a reduction of cells in the G1 phase while cells in the S phase remained constant.

Next, we investigated the association between **3b**-induced G2/M arrest and alterations in G2/M regulatory protein expression in HeLa cells. As shown in Figure 3 (panel C), **3b** caused an increase in cyclin B1 expression after 24 and 48 h, indicating an activation of the mitotic checkpoint following drug exposure. This effect was confirmed by the appearance of slower migrating forms of phosphatase cdc25c at 24 h, followed

dx.doi.org/10.1021/jm300388h | J. Med. Chem. 2012, 55, 5433−5445

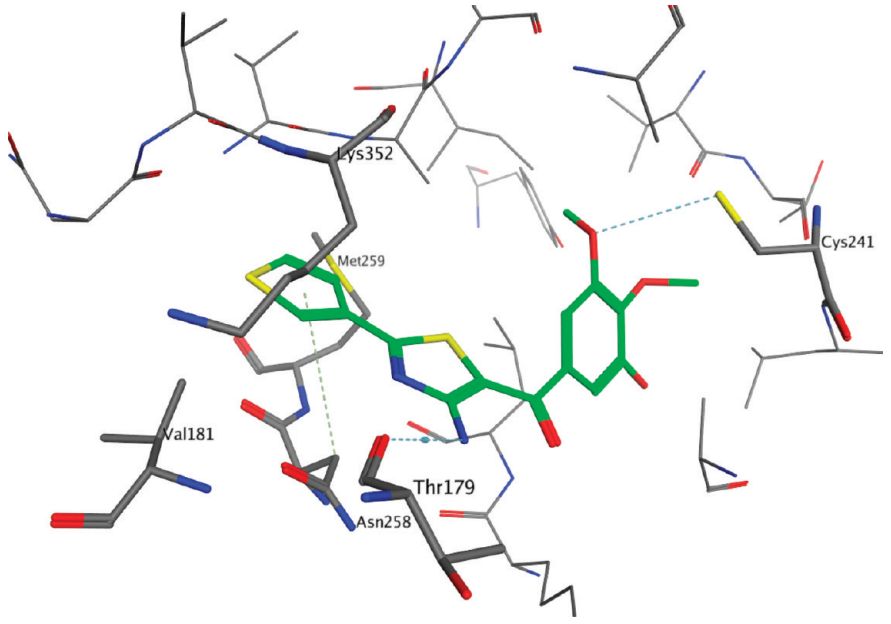

Figure 1. Proposed binding mode of **3b** in the colchicine site of β-tubulin.

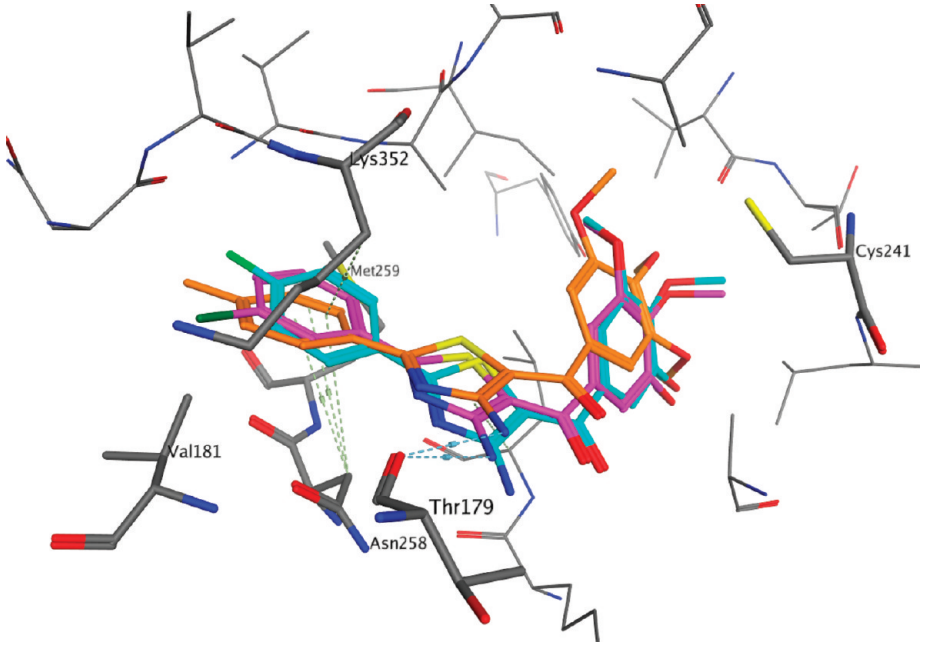

Figure 2. Putative binding mode of **3c** (in cyan), **3e** (in magenta), and **3f** (in orange) in the colchicine site of β-tubulin.

by a strong reduction at 48 h. The phosphorylation of cdc25c directly stimulates its phosphatase activity, and this is necessary to activate cdc2/cyclin B on entry into mitosis.[18] In good agreement, we also observed at 24 h of incubation, at 100 nM, a remarkable dephosphorylation at Tyr15 of cdc2 kinase, and this effect, although less pronounced, was also present after 48 h of incubation.

Compound 3b Induced Apoptosis. To evaluate the mode of cell death induced by compound **3b**, we performed a biparametric cytofluorimetric analysis using propidium iodide (PI) and annexin-V-FITC, which stain DNA and phosphatidylserine (PS) residues, respectively.

After treatment with **3b** at 50 or 100 nM for 24 or 48 h, HeLa cells were labeled with the two dyes, and the resulting red (PI) and green (FITC) fluorescence was monitored by flow cytometry. As shown in Figure 4 (panel A), **3b** caused a significant induction of apoptotic cells after 24 h. The percentage of annexin-V positive cells then further increased at 48 h (Figure 4, panel B). These findings prompted us to further investigate the apoptotic process after treatment of cells with **3b**.

Compound 3b Induced Mitochondrial Depolarization and ROS Production. Mitochondria play an essential role in the propagation of apoptosis.[19] It is well established that, at an early stage, apoptotic stimuli alter the mitochondrial transmembrane potential ($\Delta\psi_{mt}$). $\Delta\psi_{mt}$ was monitored by the fluorescence of the dye JC-1.[20] Treated HeLa cells in the presence of **3b** (50 and 100 nM) exhibited a marked shift in fluorescence compared with control cells, indicating depolarization of the mitochondrial membrane potential (data not shown). Following treatment, the percentage of cells with low $\Delta\psi_{mt}$

dx.doi.org/10.1021/jm300388h | J. Med. Chem. 2012, 55, 5433−5445

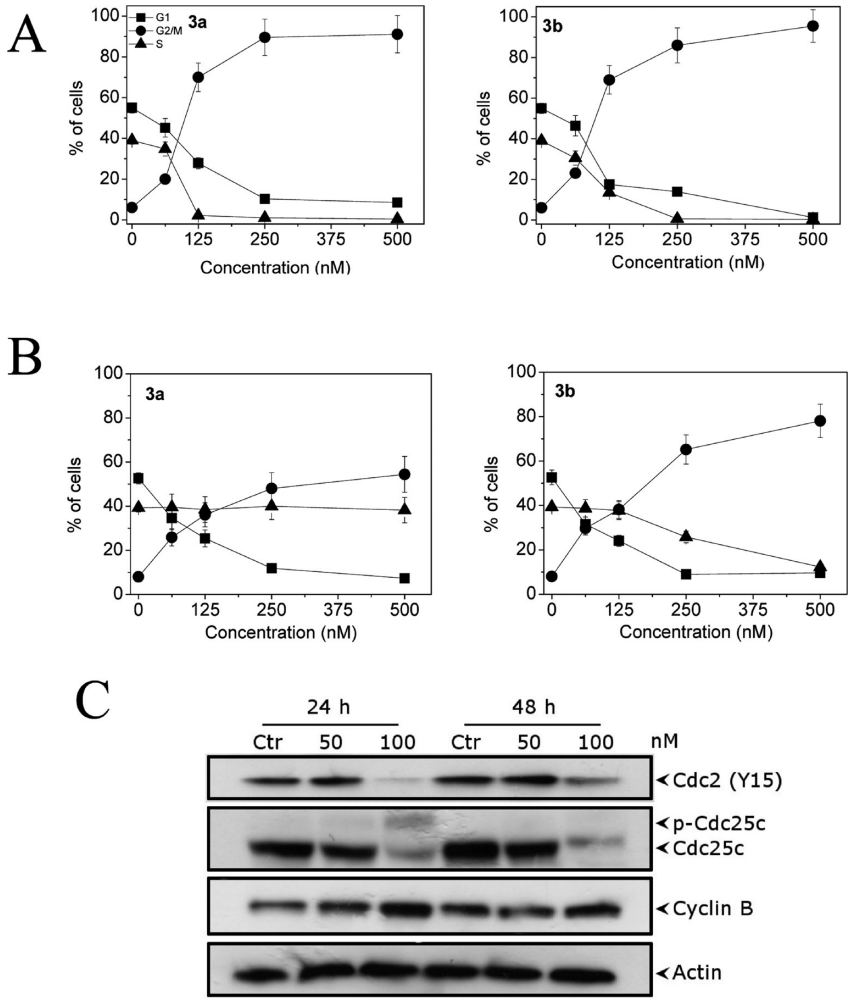

Figure 3. Effect of compounds **3a** and **3b** on cell cycle phase arrest in HeLa (panel A) and Jurkat cells (panel B). Cells were treated with different concentrations of **3a** or **3b**, as indicated, ranging from 62.5 to 500 nM for 24 h. Then, the cells were fixed and stained with PI to analyze DNA content by flow cytometry. Data are presented as the mean ± SEM of three independent experiments. Panel C: effect of **3b** on some G2/M regulatory proteins. HeLa cells were treated for 24 or 48 h with the indicated concentration of the compound. The cells were harvested and lysed for the detection of cyclin B, p-Cdc2^{Y15}, and Cdc25c expression by Western blot analysis. To ensure equal protein loading, each membrane was stripped and reprobed with anti-β-actin antibody.

increased in a time-dependent fashion (Figure 5, panel A). The disruption of $\Delta\psi_{mt}$ is associated with the appearance of annexin-V positivity in the treated cells when they are in an early apoptotic stage. In fact, the dissipation of $\Delta\psi_{mt}$ is characteristic of apoptosis and has been observed with both microtubule stabilizing and destabilizing agents, including **1**, in different cell types.[18]

Mitochondrial membrane depolarization is associated with mitochondrial production of ROS.[21] Therefore, we investigated whether ROS production increased after treatment with the test compounds. We utilized the two fluorescence indicators hydroethidine (HE) and 2,7-dichlorodihydrofluorescein diacetate (H_2-DCFDA).[22] The results are presented in Figure 5, panels B and C, which show that **3b** induced the production of significant amounts of ROS in comparison with control cells, in agreement with the dissipation of $\Delta\psi_{mt}$ described above.

Effect of 3b on Bcl-2 and Bax Expression and Caspase-3 Activation. We evaluated the activity of caspase-3 after treatment of HeLa cells with **3b** since this enzyme is essential for the propagation of the apoptotic signal after exposure to many antimitotic compounds.[23] We observed a clear activation of caspase-3, as well as cleavage of the caspase-3 substrate PARP after 24 and 48 h of **3b** exposure (Figure 6). In addition, after a 48 h exposure to 100 nM, we also found an increase in the expression of phospho-γH2AX, a well-known marker for cellular DNA double strand breaks.[24] This suggests that DNA damage probably occurred in the unsegregated chromosomes resulting from the stalled replication caused by compound **3b**. There is increasing evidence that regulation of the Bcl-2 family of protein shares the signaling pathways induced by antimicrotubule compounds.[18,25] The proteins of the Bcl family play a major role in controlling apoptosis through the regulation of mitochondrial processes and the release of mitochondrial proapoptotic molecules that are important for the cell death pathway.[18] Our results (Figure 6) showed that the expression of the antiapoptotic protein Bcl-2 was strongly reduced after 24 h of treatment with 100 nM **3b** and after 48 h with either 50 or 100 nM **3b**. In contrast, expression of Bax, a proapoptotic protein of the Bcl-2 family, was unchanged.

***In Vitro* Evaluation of Antivascular Activity of 3b.** Many studies have shown that most microtubule binding drugs possess vascular disrupting activity, and such data suggest that this class of drugs could be useful as antiangiogenic compounds.[9,10] In this context, CA-4 and its analogues in clinical

dx.doi.org/10.1021/jm300388h | J. Med. Chem. 2012, 55, 5433−5445

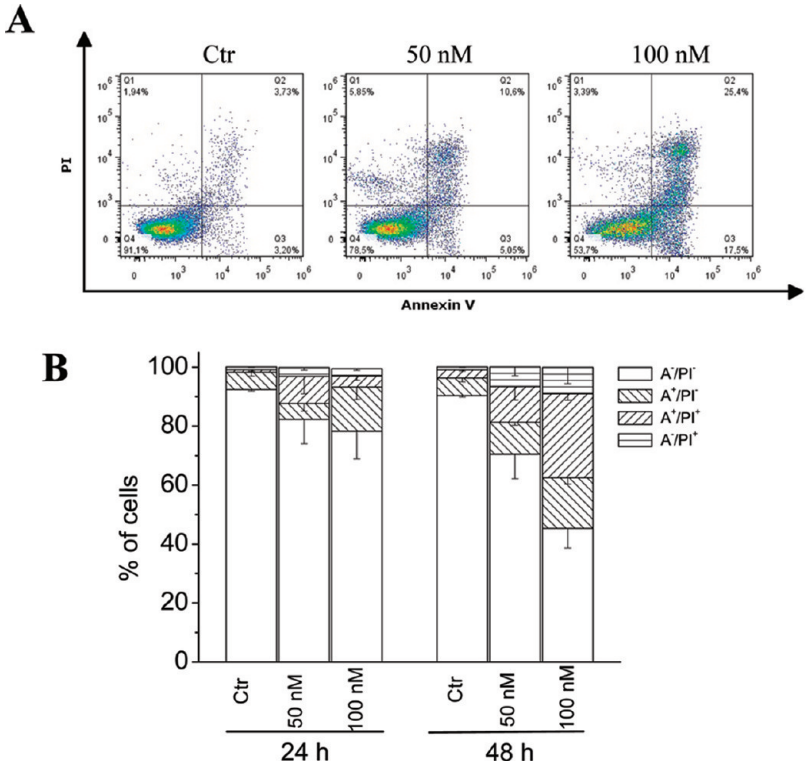

Figure 4. Panel A: representative flow cytometric histograms of apoptotic HeLa cells after 48 h treatment with **3b**. The cells were harvested and labeled with annexin-V-FITC and PI and analyzed by flow cytometry. Panel B: percentage of cells found in the different regions of the biparametric histograms after incubation with **3b** for 24 or 48 h. Data are expressed as the mean ± SEM for five independent experiments.

development have been shown to quickly and selectively shut down the blood flow of tumors.[26,27] The effect is thought to be mediated by inducing endothelial cell shape change, possibly through disruption of microtubule dynamics.[9] We tested **3b** for its ability to induce rapid endothelial cell shape changes using a human umbilical vein endothelial cell (HUVEC) culture assay. We first investigated the effects of **3b** on endothelial cell migration using an *in vitro* scratch assay.[28] We scraped confluent monolayers of HUVECs to clear space for motile cells to move into. As shown in Figure 7 (panel A), we observed that after 24 h nontreated cells migrated to completely fill the area that was initially scraped. In contrast, **3b** significantly inhibited HUVEC migration in a concentration and time dependent manner (Figure 7, panels A and B).

We also tested the effects of **3b** in a tube formation assay. After being seeded on Matrigel, HUVECs form a rich meshwork of branching capillary-like tubules with multicentric junctions. After just 1 h in different concentrations (100–500 nM) of **3b**, the capillary-like tubes were interrupted. At the two higher concentrations of **3b**, most cells were spherical and either isolated or aggregated in small clumps (Figure 7, panel C). Quantitative image analysis (Figure 7, panel D) showed that **3b** markedly decreased in a concentration dependent manner both dimensional (percent of area covered by HUVECs, total length per field) and topological parameters (number of mesh per field, number of branching points) of the capillary-like network.

To evaluate if the inhibition of cell migration and tube formation was due to a cytotoxic action of **3b**, we analyzed cell proliferation of the HUVECs by the MTT assay. The calculated GI_{50} after 72 h was 4.4 ± 0.9 μM, indicating that this compound inhibited proliferation of these cells only at concentrations higher than that required for the inhibition of cell migration and tube formation. Altogether, these preliminary observations suggest that **3b**, like CA-4, would most likely cause severe vascular disruption *in vitro*, although at a concentration higher than that of CA-4,[26,27] and warrant further studies to evaluate in depth its vascular disrupting properties.

***In Vivo* Antitumor Activity of Compound 3b.** To evaluate the *in vivo* antitumor activity of **3b**, human colon adenocarcinoma xenografts were established by subcutaneous injection of HT29 cells into the backs of nude mice. Once the HT-29 xenografts reached a size of ~300 mm^3, 12 mice were randomly assigned to one of two groups. In one of the groups, compound **3b** dissolved in DMSO was injected intraperitoneally at doses of 100 mg/kg. The drug, as well as the vehicle control, were administered three times a week for one week. As shown in Figure 8 (panel A), compound **3b** caused a significant reduction in tumor growth (58%, $p < 0.01$) as compared with the administration of vehicle only.

During the whole treatment period, no significant weight changes or macroscopic signs of toxicity occurred in the treated animals (Figure 8, panel B) suggesting that the administration of **3b** was well tolerated.

■ CONCLUSIONS

The structural refinement of compound **2a** led to the discovery of a novel series of synthetic inhibitors of tubulin polymerization with general structure **3**, based on the 2-aryl/heteroaryl-4-amino-5-(3′,4′,5′-trimethoxybenzoyl)thiazole molecular skeleton, prepared in a one-step procedure by Liebeskind–Srogl conditions starting from an easily accessible building block **5** bearing an unprotected amino group function. The antiproliferative activity of these compounds was highly dependent

dx.doi.org/10.1021/jm300388h | J. Med. Chem. 2012, 55, 5433–5445

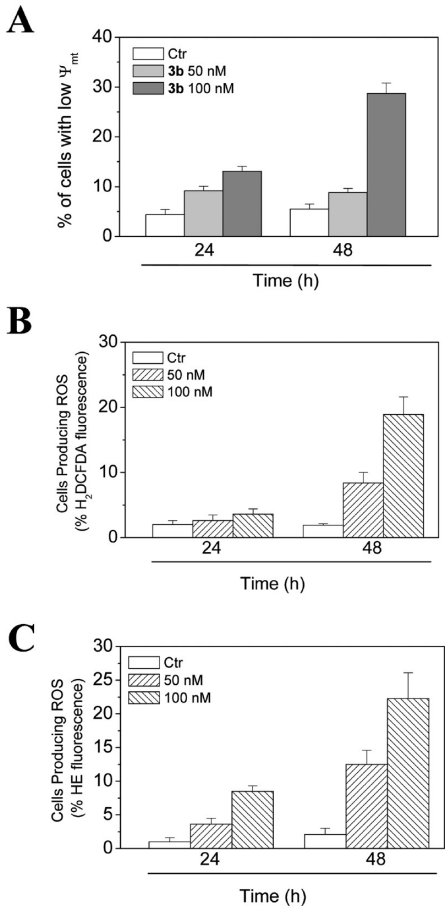

Figure 5. Assessment of HeLa mitochondrial dysfunction after treatment with compound **3b**. Panel A: induction of the loss of mitochondrial membrane potential after 24 or 48 h incubations with compound **3b**. Cells were stained with the fluorescent probe JC-1 and analyzed by flow cytometry. Data are expressed as the mean ± SEM for three independent experiments. Panels B and C: mitochondrial production of ROS in HeLa cells. After 24 or 48 h incubations with **3b**, cells were stained with H_2-DCFDA (panel B) or HE (panel C) and analyzed by flow cytometry. Data are expressed as the mean ± SEM of three independent experiments.

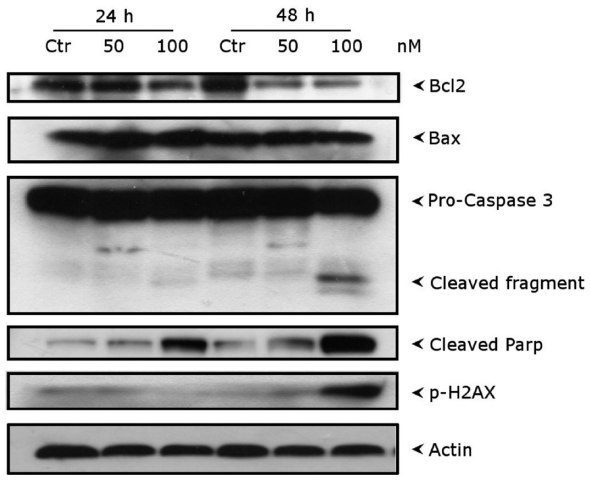

Figure 6. Western blot analysis for caspase-3 activation, PARP cleavage, and the expression of Bcl-2, Bax, and histone γH2AX in HeLa cells. The cells were treated with the indicated concentration of **3b** for 24 or 48 h. Whole cell lysates were subjected to SDS–PAGE, followed by blotting with the appropriate antibody or an antiactin antibody.

on the structure modifications on the 2-position of the thiazole ring. The substituents examined included phenyl, 3-thienyl, and substituted phenyls bearing EWGs or ERGs.

The study revealed that phenyl (**3a**) and 3-thienyl (**3b**) thiazole derivatives exhibited improved growth inhibition activity as compared with the activity of the corresponding pyrrolidine analogue **2a**. Moreover, compounds **3a** and **3b** exhibited the best antiproliferative activity among the compounds synthesized in this study.

Overall, these compounds had greater potency than **1** against MCF-7 and HT-29 cells, comparable activity against HeLa and A549 cells, and less activity against HL-60 and Jurkat cells. Comparing **3a** with the bioisosteric 3-thienyl derivative **3b**, the latter was less active than **3a** only in MCF-7 cells. In general, the introduction of EWGs and ERGs reduced activity compared with the unsubstituted phenyl derivative **3a**, with no clear difference in effect on potency between EWGs and ERGs. At the *para*-position, only fluorine and methyl were tolerated, while the introduction of all other EWGs (Cl, NO_2, and CF_3) and ERGs (Et, $C(CH_3)_3$; OCF_3 and OEt) significantly reduced antiproliferative activity. For methoxy and chloro substituents, their position on the phenyl ring had a profound influence on potency. Moving the chloro group from the *para*- to the *meta*-position (compounds **3d** and **3e**, respectively) led to a dramatic increase in antiproliferative activity. The same effect was observed for the methoxy substituent (**3j** vs **3k**). In contrast, the insertion of an additional methoxy group, to yield the *m*,*p*-dimethoxy derivative **3l**, substantially reduced antiproliferative activity. These substituent effects are probably caused by increased steric hindrance in the colchicine site, preventing efficient binding, as observed in the molecular modeling studies. Thus, a selected, single, and small EWG or ERG could be placed on the phenyl ring with relatively minor effects on antiproliferative activity, but no modification improved activity relative to the unsubstuted phenyl or 3-thienyl derivatives **3a** and **3b**, respectively. Moreover, several compounds, such as **3c** and **3f**, characterized by the presence of substituents with opposite electronic effects showed approximately the same potency.

We identified tubulin as the molecular target of the compounds since derivatives **3a** and **3b**, with the greatest inhibitory effects on cell growth, strongly inhibited tubulin assembly and the binding of colchicine to tubulin. Their potency for inhibition of tubulin polymerization was comparable with that of the reference compound **1**.

We also showed that **3b** had cellular effects typical for microtubule interacting agents, causing accumulation of cells in the G2/M phase of the cell cycle. Further studies showed that **3b** was a potent inducer of apoptosis in HeLa cells. Apoptosis induced by antimitotic agents has been associated with alterations in a variety of cellular signaling pathways. As with many antimitotic drugs, compound **3b** induced Bcl-2 down-regulation after a 24 h treatment. Bcl-2 prevents the initiation of the cellular apoptotic program by stabilizing mitochondrial permeability. Our results confirmed that the induction of apoptosis by **3b** was associated with down-regulation of Bcl-2, dissipation of the mitochondrial transmembrane potential, and activation of caspase-3, which is coupled with terminal events of apoptosis, such as PARP cleavage. These effects were in good agreement with the cytotoxic potency of this compound and occur at lower concentrations than was observed with compound **2a**.[8] Compound **3b** was also active in

dx.doi.org/10.1021/jm300388h | J. Med. Chem. 2012, 55, 5433–5445

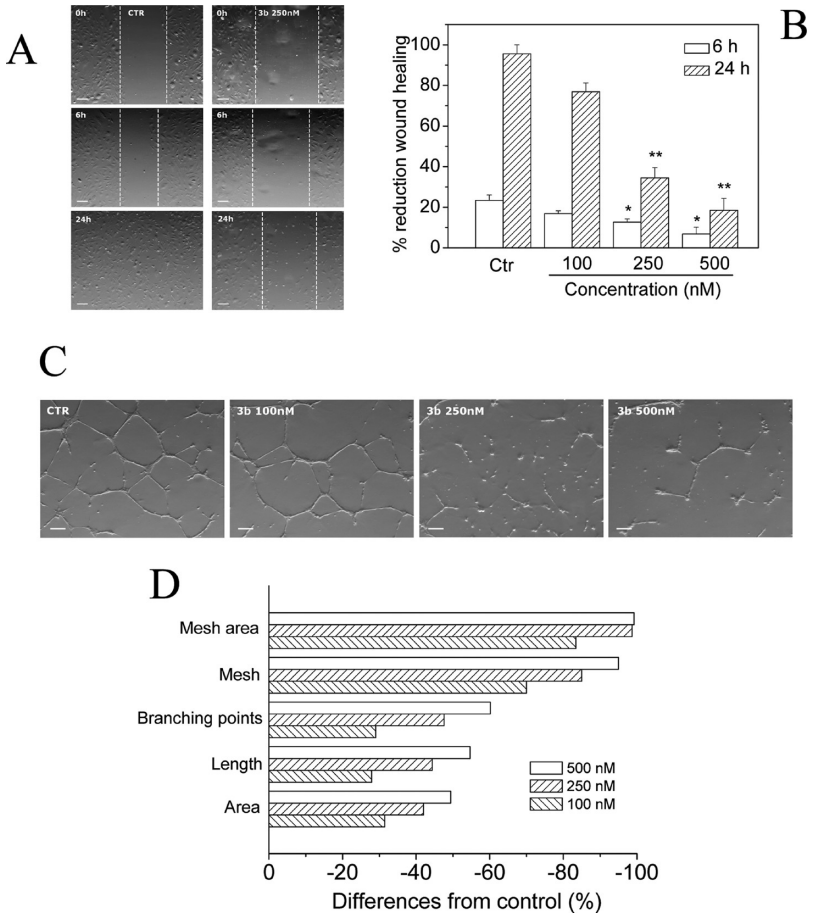

Figure 7. Antivascular activity of compound **3b**. Panel A: **3b** inhibits HUVEC migration. Confluent HUVEC monolayers were scratch wounded. The cells were treated with various concentrations of **3b** and at different times cells were photographed (40× magnification). The dotted lines define the areas lacking cells. Panel B: the graph shows the quantitative effect of **3b**. Data are presented as the mean ± SEM of three independent experiments. $*p < 0.05$, $**p < 0.01$ vs control. Panel C: inhibition of endothelial cell capillary-like tubule formation by **3b**. Tubule formation on Matrigel was performed as described in Materials and Methods. Representative pictures (40× magnification) of HUVECs treated with the indicated concentrations of **3b** for 3 h. Panel D: the graph shows the quantitative effects of **3b** on the dimensional and topological parameters of the HUVEC network.

suppressing the growth of drug resistant cells, and even more importantly, it had significant *in vivo* activity in a colon cancer xenograft model. Finally, preliminary experiments were performed to assess the potential antivascular activity of compound **3b**. The ability of this compound to inhibit HUVEC migration and to destroy pre-established vessels formed by HUVECs is consistent with antivascular activity and warrants further testing in *in vivo* cancer models.

EXPERIMENTAL SECTION

Chemistry. *Materials and Methods.* ^{1}H and ^{13}C NMR spectra were recorded on a Bruker AC 200 and Varian 400 Mercury Plus spectrometer, respectively. Chemical shifts (δ) are given in ppm, and the spectra were recorded in appropriate deuterated solvents, as indicated. Infrared spectra were recorded on a Perkin-Elmer Spectrum 100 FTIR spectrometer using the ATR technique. The main bands are given in cm^{-1}. Positive-ion electrospray ionization (ESI) mass spectra were recorded on a double-focusing Finnigan MAT 95 instrument with BE geometry. Melting points (mp) were determined on a Buchi-Tottoli apparatus and are uncorrected. All products reported showed ^{1}H NMR spectra in agreement with the assigned structures. The purity of tested compounds was determined by combustion elemental analyses conducted by the Microanalytical Laboratory of the Chemistry Department of the University of Ferrara with a Yanagimoto MT-5 CHN recorder elemental analyzer. All tested compounds yielded data consistent with a purity of at least 95% as compared with the theoretical values. All reactions were carried out under an inert atmosphere of dry nitrogen, unless otherwise indicated. Standard syringe techniques were used for transferring dry solvents. Reaction courses and product mixtures were routinely monitored by TLC on silica gel (precoated F_{254} Merck plates), and compounds were visualized with aqueous $KMnO_4$. Flash chromatography was performed using 230−400 mesh silica gel and the indicated solvent system. Organic solutions were dried over anhydrous Na_2SO_4. Arylboronic acids are commercially available and used as received. All chemicals and reagents were purchased from Aldrich (Sigma-Aldrich) or Lancaster (Alfa Aesar, Johnson Matthey Company).

*Synthesis of (4-Amino-2-(methylthio)thiazol-5-yl)(3,4,5-trimethoxyphenyl)methanone (**5**).* To a stirred suspension of $Na_2S{\cdot}9H_2O$ (1.2 g., 5 mmol) in DMF (7 mL), dimethyl cyanodithioimidocarbonate **4** (730 mg, 5 mmol) dissolved in DMF (5 mL) was added, and the mixture was heated at 70 °C for 2 h. Then, 2-bromo-1-(3,4,5-trimethoxyphenyl)ethanone (2.89 g., 10 mmol) dissolved in DMF (5 mL) was slowly added dropwise at 50 °C. The mixture was heated at 50 °C for 2 h, and potassium carbonate was added (690 mg, 10 mmol). The reaction was stirred at 50 °C for an additional hour. The mixture was poured onto water (100 mL) with stirring. When a yellow precipitate appeared, it was filtered, washed with water, and dried at room temperature until a constant weight was reached. The isolated solid was purified by stirring in petroleum ether for 1 h and filtered to afford (**5**) as a yellow solid. Yield 52%,

dx.doi.org/10.1021/jm300388h | J. Med. Chem. 2012, 55, 5433−5445

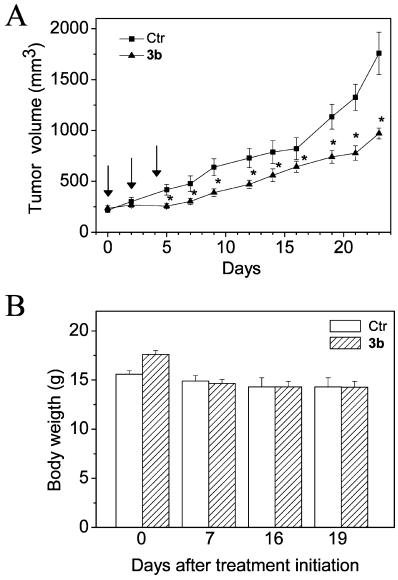

Figure 8. Inhibition of human xenograft growth *in vivo* by compound **3b**. Panel A: HT29 tumor-bearing nude mice were administered either vehicle control or 100 mg/kg of **3b** in vehicle intraperitoneally on days 0, 2, and 4 (indicated by arrows). The figure shows the tumor volume (panel A) and body weight (panel B) recorded at the indicated days after treatments. Data are expressed as the mean ± SEM of tumor volume and body weight at each time point for six animals per group. *$p < 0.01$ vs the control.

mp 130–132 °C. ^{1}H NMR ($CDCl_3$) δ: 2.67 (s, 3H), 3.90 (s, 3H), 3.91 (s, 6H), 6.82 (bs, 2H), 7.03 (s, 2H). ^{13}C NMR (100 MHz, $CDCl_3$) δ: 13.6, 56.3 (2C), 61.0, 104.7 (2C), 105.2, 137.1, 139.9, 153.0 (2C), 165.2, 172.2, 183.3. IR (ATR) ν: 3293, 1594, 1532, 1455, 1407, 1337, 1116, 998, 736.

*General Procedure for the Synthesis of (4-Amino-2-arylthiazol-5-yl)(3,4,5-trimethoxyphenyl)methanone (**3a–o**).* To a stirred solution of (4-amino-2-(methylthio)thiazol-5-yl)(3,4,5-trimethoxyphenyl)-methanone **5** (170 mg, 0.5 mmol) in THF (10 mL) were subsequently added the appropriate arylboronic acid (1 mmol), TFP (19 mg, 0.08 mmol), and CuTC (0.125 g, 0.65 mmol). The reaction vessel was flushed with argon, then Pd_2-dba_3·$CHCl_3$ (20 mg, 0.02 mmol) was added, and the reaction mixture was stirred at 70 °C for 18 h. After cooling, the mixture was diluted with dichloromethane (5 mL) and filtered through Celite, and the filtrate was evaporated. The residue was dissolved in dichloromethane (15 mL), and the mixture was washed with 25% aqueous ammonia (2 × 5 mL). The organic layer was dried and the residue after evaporation purified by silica gel column chromatography (gradient of petroleum ether and ethyl acetate), giving the desired product.

*(4-Amino-2-phenylthiazol-5-yl)(3,4,5-trimethoxyphenyl)-methanone (**3a**).* Following the general procedure, the crude residue, purified by flash chromatography using ethyl acetate/petroleum ether 4:6 (v/v) as eluent, furnished **3a** as a yellow solid (52% yield); mp 156–158 °C. ^{1}H NMR ($CDCl_3$) δ: 3.93 (s, 6H), 3.94 (s, 3H), 6.94 (bs, 2H), 7.11 (s, 2H), 7.48 (m, 3H), 7.95 (dd, J = 8.0 and 2.0 Hz, 2H). ^{13}C NMR (100 MHz, $CDCl_3$) δ: 56.3 (2C), 60.9, 105.2 (2C), 108.9, 127.0 (2C), 129.3 (2C), 131.2, 132.4, 133.4, 135.7, 141.1, 153.2 (2C), 163.7, 186.4. IR (ATR) ν: 3384, 1620, 1578, 1450, 1411, 1337, 1127, 999, 817, 760. MS (ESI): $[M]^+$ = 370.7. Anal. ($C_{19}H_{18}N_2O_4S$) C, H, N.

*(4-Amino-2-(thiophen-3-yl)thiazol-5-yl)(3,4,5-trimethoxyphenyl)-methanone (**3b**).* Following the general procedure, the crude residue, purified by flash chromatography using ethyl acetate/petroleum ether 1:1 (v/v) as eluent, furnished **3b** as a yellow solid (58% yield); mp 198–200 °C. ^{1}H NMR ($CDCl_3$) δ: 3.92 (s, 6H), 3.93 (s, 3H), 6.98 (bs, 2H), 7.09 (s, 2H), 7.42 (d, J = 8.4 Hz, 1H), H), 7.51 (d, J = 8.4 Hz, 1H), 8.03 (s, 1H). ^{13}C NMR (100 MHz, $CDCl_3$) δ: 56.3 (2C), 60.9, 101.4, 105.2 (2C), 125.9, 127.6, 133.9, 134.2, 135.8, 141.0, 153.1 (2C), 164.0, 166.4, 186.3. IR (ATR) ν: 3377, 1614, 1577, 1445, 1408, 1338, 1234, 1125, 989, 819, 763. MS (ESI): $[M]^+$ = 376.8. Anal. ($C_{17}H_{16}N_2O_4S_2$) C, H, N.

*(4-Amino-2-(4-fluorophenyl)thiazol-5-yl)(3,4,5-trimethoxyphenyl)methanone (**3c**).* Following the general procedure, the crude residue, purified by flash chromatography using ethyl acetate/petroleum ether 6:4 (v/v) as eluent, furnished **3c** as a yellow solid (49% yield); mp 196–197 °C. ^{1}H NMR ($CDCl_3$) δ: 3.92 (s, 6H), 3.93 (s, 3H), 7.02 (bs, 2H), 7.12 (s, 2H), 7.19 (m, 2H), 7.94 (m, 2H). ^{13}C NMR (100 MHz, $CDCl_3$) δ: 56.4 (2C), 61.0, 102.4, 105.2 (2C), 116.3, 116.6, 128.5, 129.1, 129.2, 135.9, 141.0, 153.2 (2C), 163.8, 165.3 (d, J = 253.3 Hz), 170.8, 186.5. IR (ATR) ν: 3262, 1620, 1578, 1450, 1408, 1337, 1236, 1129, 994, 813, 759. MS (ESI): $[M]^+$ = 388.9. Anal. ($C_{19}H_{17}FN_2O_4S$) C, H, N.

*(4-Amino-2-(4-chlorophenyl)thiazol-5-yl)(3,4,5-trimethoxyphenyl)methanone (**3d**).* Following the general procedure, the crude residue, purified by flash chromatography using ethyl acetate/petroleum ether 6:4 (v/v) as eluent, furnished **3d** as a yellow solid (48% yield); mp 146–148 °C. ^{1}H NMR ($CDCl_3$) δ: 3.92 (s, 6H), 3.93 (s, 3H), 6.82 (bs, 2H), 7.10 (s, 2H), 7.42 (d, J = 8.8 Hz, 2H), 7.88 (d, J = 8.8 Hz, 2H). ^{13}C NMR (100 MHz, $CDCl_3$) δ: 56.4 (2C), 61.1, 102.6, 105.3 (2C), 110.2, 128.1 (2C), 129.5 (2C), 130.7, 135.9, 138.2, 153.2 (2C), 164.8, 170.7, 186.6. IR (ATR) ν: 3313, 2930, 1614, 1572, 1414, 1335, 1129, 818, 758. MS (ESI): $[M]^+$ = 404.9. Anal. ($C_{19}H_{17}ClN_2O_4S$) C, H, N.

*(4-Amino-2-(3-chlorophenyl)thiazol-5-yl)(3,4,5-trimethoxyphenyl)methanone (**3e**).* Following the general procedure, the crude residue, purified by flash chromatography using ethyl acetate/petroleum ether 6:4 (v/v) as eluent, furnished **3e** as a yellow solid (58% yield); mp 185–186 °C. ^{1}H NMR ($CDCl_3$) δ: 3.93 (s, 6H), 3.94 (s, 3H), 6.84 (bs, 2H), 7.11 (s, 2H), 7.35 (d, J = 7.8 Hz, 2H), 7.46 (dt, J = 7.2 and 1.6 Hz, 1H), 7.83 (dt, J = 7.2 and 1.6 Hz, 1H), 7.96 (t, J = 1.4 Hz, 1H). ^{13}C NMR (100 MHz, $CDCl_3$) δ: 56.3 (2C), 60.9, 102.7, 105.2 (2C), 124.9, 126.7, 130.4, 131.7, 133.9, 135.3, 135.8, 141.0, 153.1 (2C), 164.7, 170.2, 186.6. IR (ATR) ν: 3307, 1614, 1577, 1339, 1236, 1133, 992, 820, 761. MS (ESI): $[M]^+$ = 404.9. Anal. ($C_{19}H_{17}ClN_2O_4S$) C, H, N.

*(4-Amino-2-p-tolylthiazol-5-yl)(3,4,5-trimethoxyphenyl)-methanone (**3f**).* Following the general procedure, the crude residue, purified by flash chromatography using ethyl acetate/petroleum ether 1:1 (v/v) as eluent, furnished **3f** as a yellow solid (45% yield); mp 130–132 °C. ^{1}H NMR ($CDCl_3$) δ: 2.41 (s, 3H), 3.92 (s, 6H), 3.93 (s, 3H), 6.84 (bs, 2H), 7.11 (s, 2H), 7.26 (d, J = 8.2 Hz, 2H), 7.84 (d, J = 8.2 Hz, 2H). ^{13}C NMR (100 MHz, $CDCl_3$) δ: 21.7, 56.3 (2C), 60.9, 101.9, 105.2 (2C), 126.9 (2C), 129.2, 129.9 (2C), 135.9, 140.9, 143.0, 153.1 (2C), 164.4, 172.2, 186.3. IR (ATR) ν: 3314, 2928, 1612, 1574, 1412, 1335, 1235, 1128, 991, 816, 759. MS (ESI): $[M]^+$ = 384.9. Anal. ($C_{20}H_{20}N_2O_4S$) C, H, N.

*(4-Amino-2-(4-ethylphenyl)thiazol-5-yl)(3,4,5-trimethoxyphenyl)-methanone (**3g**).* Following the general procedure, the crude residue, purified by flash chromatography using ethyl acetate/petroleum ether 1:1 (v/v) as eluent, furnished **3g** as a yellow solid (56% yield); mp 86–87 °C. ^{1}H NMR ($CDCl_3$) δ: 1.26 (t, J = 7.2 Hz, 3H), 2.69 (q, J = 7.2 Hz, 2H), 3.92 (s, 6H), 3.93 (s, 3H), 6.94 (bs, 2H), 7.12 (s, 2H), 7.29 (d, J = 8.2 Hz, 2H), 7.88 (d, J = 8.2 Hz, 2H). ^{13}C NMR (100 MHz, $CDCl_3$) δ: 15.3, 29.0, 56.4 (2C), 61.0, 102.2, 105.2 (2C), 127.6 (2C), 133.9, 135.9 (2C), 136.1, 140.9, 149.0, 153.1 (2C), 165.1, 172.6, 186.5. IR (ATR) ν: 3273, 2931, 1621, 1574, 1453, 1412, 1334, 1237, 1128, 1004, 820, 759. MS (ESI): $[M]^+$ = 398.8. Anal. ($C_{21}H_{22}N_2O_4S$) C, H, N.

*(4-Amino-2-(4-tert-butylphenyl)thiazol-5-yl)(3,4,5-trimethoxyphenyl)methanone (**3h**).* Following the general procedure, the crude residue, purified by flash chromatography using ethyl acetate/petroleum ether 4:6 (v/v) as eluent, furnished **3h** as a yellow solid (54% yield); mp 66–68 °C. ^{1}H NMR ($CDCl_3$) δ: 1.35 (s, 9H), 3.93 (s, 6H), 3.94 (s, 3H), 6.91 (bs, 2H), 7.12 (s, 2H), 7.47 (d, J = 8.4 Hz, 2H), 7.89 (d, J = 8.4 Hz, 2H). ^{13}C NMR (100 MHz, $CDCl_3$) δ: 31.3 (3C), 35.2, 56.3 (2C), 61.1, 105.3 (2C), 110.9, 125.0, 126.2 (2C), 126.8 (2C), 128.5, 136.1, 142.1, 153.2 (2C), 155.9, 164.9, 186.5. IR (ATR) ν: 2958, 1574, 1402, 1334, 1233, 1124, 1000, 818, 763. MS (ESI): $[M]^+$ = 426.7. Anal. ($C_{23}H_{26}N_2O_4S$) C, H, N.

*(4-Amino-2-(4-trifluoromethylphenyl)thiazol-5-yl)(3,4,5-trimethoxyphenyl)methanone (**3i**).* Following the general procedure, the crude residue, purified by flash chromatography using ethyl acetate/petroleum ether 4:6 (v/v) as eluent, furnished **3i** as a yellow solid (56% yield); mp 166−167 °C. ^{1}H NMR ($CDCl_3$) δ: 3.93 (s, 6H), 3.94 (s, 3H), 6.86 (bs, 2H), 7.11 (s, 2H), 7.71 (d, J = 8.2 Hz, 2H), 8.05 (d, J = 8.2 Hz, 2H). ^{13}C NMR (100 MHz, $CDCl_3$) δ: 56.4 (2C), 61.0, 103.2, 105.3 (2C), 123.7 (q, J = 271.5 Hz), 126.2 (2C), 126.4, 127.1 (2C), 133.2 (q, J = 32.7 Hz), 135.5, 135.8, 141.2, 153.2 (2C), 164.9, 169.9, 186.8. IR (ATR) ν: 3314, 2930, 1613, 1575, 1322, 1237, 1127, 1104, 1067, 845, 817, 760. MS (ESI): $[M]^+$ = 438.7. Anal. ($C_{20}H_{17}F_3N_2O_4S$) C, H, N.

*(4-Amino-2-(4-methoxyphenyl)thiazol-5-yl)(3,4,5-trimethoxyphenyl)methanone (**3j**).* Following the general procedure, the crude residue, purified by flash chromatography using ethyl acetate/petroleum ether 6:4 (v/v) as eluent, furnished **3j** as a yellow solid (46% yield); mp 196−198 °C. ^{1}H NMR ($CDCl_3$) δ: 3.87 (s, 3H), 3.92 (s, 6H), 3.93 (s, 3H), 6.82 (bs, 2H), 6.93 (d, J = 8.0 Hz, 2H), 7.11 (s, 2H), 7.90 (d, J = 8.0 Hz, 2H). ^{13}C NMR (100 MHz, $CDCl_3$) δ: 55.8, 56.5 (2C), 61.2, 101.8, 105.3 (2C), 114.8 (2C), 124.9, 129.0 (2C), 136.3, 141.1, 153.2 (2C), 163.1, 164.8, 172.3, 186.4. IR (ATR) ν: 3298, 1573, 1397, 1259, 1124, 1004, 825, 756. MS (ESI): $[M]^+$ = 400.8. Anal. ($C_{20}H_{20}N_2O_5S$) C, H, N.

*(4-Amino-2-(3-methoxyphenyl)thiazol-5-yl)(3,4,5-trimethoxyphenyl)methanone (**3k**).* Following the general procedure, the crude residue, purified by flash chromatography using ethyl acetate/petroleum ether 1:1 (v/v) as eluent, furnished **3k** as an orange solid (47% yield); mp 167−168 °C. ^{1}H NMR ($CDCl_3$) δ: 3.87 (s, 3H), 3.92 (s, 6H), 3.93 (s, 3H), 6.84 (bs, 2H), 7.07 (m, 1H), 7.11 (s, 2H), 7.36 (t, J = 7.2 Hz, 1H), 7.54 (m, 2H). ^{13}C NMR (100 MHz, $CDCl_3$) δ: 55.7, 56.4 (2C), 61.1, 105.3 (2C), 111.7, 118.7, 119.5, 130.5, 132.9. 135.8, 141.1, 153.2 (2C), 160.2, 162.8, 170.5, 171.8, 186.5. IR (ATR) ν: 3275, 1615, 1579, 1503, 1409, 1337, 1235, 1129, 994, 826, 769, 674. MS (ESI): $[M]^+$ = 400.8. Anal. ($C_{20}H_{20}N_2O_5S$) C, H, N.

*(4-Amino-2-(3,4-dimethoxyphenyl)thiazol-5-yl)(3,4,5-trimethoxyphenyl)methanone (**3l**).* Following the general procedure, the crude residue, purified by flash chromatography using ethyl acetate/petroleum ether 2:8 (v/v) as eluent, furnished **3l** as a red solid (45% yield); mp 176−177 °C. ^{1}H NMR ($CDCl_3$) δ: 3.92 (s, 6H), 3.93 (s, 3H), 3.95 (s, 3H), 3.98 (s, 3H), 6.80 (bs, 2H), 6.88 (d, J = 8.8 Hz, 1H), 7.10 (s, 2H), 7.51 (d, J = 8.8 Hz, 1H), 7.54 (s, 1H). ^{13}C NMR (100 MHz, $CDCl_3$) δ: 56.3, 56.5 (2C), 61.1, 62.3, 100.4, 105.2, 107.2 (2C), 107.6, 109.8, 111.4, 121.5, 135.3, 141.3, 149.7, 153.2 (2C), 169.2, 170.9, 186.0. IR (ATR) ν: 2933, 1579, 1454, 1411, 1333, 1261, 1121, 1101, 1006, 799. MS (ESI): $[M]^+$ = 431.0. Anal. ($C_{21}H_{22}N_2O_6S$) C, H, N.

*(4-Amino-2-(4-ethoxyphenyl)thiazol-5-yl)(3,4,5-trimethoxyphenyl)methanone (**3m**).* Following the general procedure, the crude residue, purified by flash chromatography using ethyl acetate/petroleum ether 6:4 (v/v) as eluent, furnished **3m** as an orange solid (44% yield); mp 185−186 °C. ^{1}H NMR ($CDCl_3$) δ: 1.44 (t, J = 7.2 Hz, 3H), 3.92 (s, 6H), 3.93 (s, 3H), 4.11 (q, J=7.2 Hz, 2H), 6.80 (bs, 2H), 6.94 (d, J = 8.6 Hz, 2H), 7.11 (s, 2H), 7.90 (d, J = 8.6 Hz, 2H). ^{13}C NMR (100 MHz, $CDCl_3$) δ: 14.8, 56.4 (2C), 61.1, 63.9, 102.0, 105.6 (2C), 115.2 (2C), 124.6, 128.9 (2C), 136.1, 141.3, 153.2 (2C), 163.1, 164.6, 172.2, 186.0. IR (ATR) ν: 2996, 1597, 1573, 1406, 1337, 1235, 1119, 104, 1006, 820, 763. MS (ESI): $[M]^+$ = 414.9. Anal. ($C_{21}H_{22}N_2O_5S$) C, H, N.

*(4-Amino-2-(4-trifluoromethoxyphenyl)thiazol-5-yl)(3,4,5-trimethoxyphenyl)methanone (**3n**).* Following the general procedure, the crude residue, purified by flash chromatography using ethyl acetate/petroleum ether 1:1 (v/v) as eluent, furnished **3n** as a yellow solid (49% yield); mp 174−176 °C. ^{1}H NMR ($CDCl_3$) δ: 3.92 (s, 6H), 3.93 (s, 3H), 6.90 (bs, 2H), 7.11 (s, 2H), 7.28 (d, J = 9.0 Hz, 2H), 7.98 (d, J = 9.0 Hz, 2H). ^{13}C NMR (100 MHz, $CDCl_3$) δ: 56.4 (2C), 61.1, 102.6, 105.3 (2C), 114.4, 120.4 (q, J = 257.8 Hz), 121.3 (2C), 128.7 (2C), 135.8, 151.9, 153.2 (2C), 162.6, 163.6, 170.1, 186.6. IR (ATR) ν: 3315, 1614, 1576, 1337, 1236, 1127, 997, 816, 759. MS (ESI): $[M]^+$ = 454.7. Anal. ($C_{20}H_{17}F_3N_2O_5S$) C, H, N.

*(4-Amino-2-(4-nitrophenyl)thiazol-5-yl)(3,4,5-trimethoxyphenyl)-methanone (**3o**).* Following the general procedure, the crude residue, purified by flash chromatography using ethyl acetate/petroleum ether 6:4 (v/v) as eluent, furnished **3o** as a red solid (42% yield); mp 234−236 °C. ^{1}H NMR ($CDCl_3$) δ: 3.93 (s, 6H), 3.94 (s, 3H), 6.92 (bs, 2H), 7.11 (s, 2H), 8.15 (d, J = 9.0 Hz, 2H), 8.31 (d, J = 9.0 Hz, 2H). ^{13}C NMR (100 MHz, $CDCl_3$) δ: 56.4 (2C), 61.1, 105.3 (2C), 106.5, 124.5 (2C), 127.6 (2C), 124.8, 135.7, 137.9, 149.4, 153.3 (2C), 160.2, 168.4, 186.9. IR (ATR) ν: 3337, 1593, 1577, 1519, 1415, 1331, 1234, 1130, 850, 816. MS (ESI): $[M]^+$ = 415.8. Anal. ($C_{19}H_{17}N_3O_6S$) C, H, N.

Antiproliferative Assays. Human T-leukemia (Jurkat) and human promyelocytic leukemia (HL-60) cells were grown in RPMI-1640 medium, (Gibco, Milano, Italy). Breast adenocarcinoma (MCF-7), human nonsmall cell lung carcinoma (A549), human cervix carcinoma (HeLa), and human colon adenocarcinoma (HT-29) cells were grown in DMEM medium (Gibco, Milano, Italy). Both media were supplemented with 115 units/mL of penicillin G (Gibco, Milano, Italy), 115 μg/mL of streptomycin (Invitrogen, Milano, Italy), and 10% fetal bovine serum (Invitrogen, Milano, Italy). LoVo^{Doxo} cells are a doxorubicin resistant subclone of LoVo cells[13] and were grown in complete Ham's F12 medium supplemented with doxorubicin (0.1 μg/mL). CEM$^{Vbl\text{-}100}$ cells are a multidrug-resistant line selected against vinblastine.[14] A549-T12 cells are a nonsmall cell lung carcinoma line exhibiting resistance to taxol.[15] They were grown in complete DMEM medium supplemented with taxol (12 nM). Stock solutions (10 mM) of the different compounds were obtained by dissolving them in DMSO. Individual wells of a 96-well tissue culture microtiter plate were inoculated with 100 μL of complete medium containing 8×10^3 cells. The plates were incubated at 37 °C in a humidified 5% CO_2 incubator for 18 h prior to the experiments. After medium removal, 100 μL of fresh medium containing the test compound at different concentrations was added to each well and incubated at 37 °C for 72 h. The percentage of DMSO in the medium never exceeded 0.25%. This was also the maximum DMSO concentration in all cell-based assays described below. Cell viability was assayed by the (3-(4,5-dimethylthiazol-2-yl)-2,5-diphenyl tetrazolium bromide test as previously described.[20] The IC_{50} was defined as the compound concentration required to inhibit cell proliferation by 50%, in comparison with cells treated with the maximum amount of DMSO (0.25%) and considered as 100% viability.

Effects on Tubulin Polymerization and on Colchicine Binding to Tubulin. To evaluate the effect of the compounds on tubulin assembly *in vitro*,[16a] varying concentrations of compounds were preincubated with 10 μM bovine brain tubulin in glutamate buffer at 30 °C and then cooled to 0 °C. After the addition of 0.4 mM GTP, the mixtures were transferred to 0 °C cuvettes in a recording spectrophotometer and warmed to 30 °C. Tubulin assembly was followed turbidimetrically at 350 nm. The IC_{50} was defined as the compound concentration that inhibited the extent of assembly by 50% after a 20 min incubation. The capacity of the test compounds to inhibit colchicine binding to tubulin was measured as described,[16b] except that the reaction mixtures contained 1 μM tubulin, 5 μM [^{3}H]colchicine, and 5 μM test compound.

Molecular Modeling. All molecular modeling studies were performed on a MacPro dual 2.66 GHz Xeon running Ubuntu 10. The tubulin structure was downloaded from the Protein Data Bank (http://www.rcsb.org/; PDB code 3HKC).[29] Hydrogen atoms were added to the protein, using the Protonate3D function of Molecular Operating Environment (MOE).[30] Ligand structures were built with MOE and minimized using the MMFF94x forcefield until a rmsd gradient of 0.05 kcal mol^{-1} Å^{-1} was reached. The docking simulations were performed using PLANTS.[31]

Flow Cytometric Analysis of Cell Cycle Distribution. For flow cytometric analysis of DNA content, 5×10^5 HeLa or Jurkat cells in exponential growth were treated with different concentrations of the test compounds for 24 or 48 h. After the incubation, the cells were collected, centrifuged, and fixed with ice-cold ethanol (70%). The cells were treated with lysis buffer containing RNase A and 0.1% Triton X-100 and stained with PI. Samples were analyzed on a Cytomic FC500 flow cytometer (Beckman Coulter). DNA histograms were analyzed using MultiCycl for Windows (Phoenix Flow Systems).

Annexin-V Assay. Surface exposure of PS on apoptotic cells was measured by flow cytometry with a Coulter Cytomics FC500

(Beckman Coulter) by adding annexin-V-FITC to cells according to the manufacturer's instructions (Annexin-V Fluos, Roche Diagnostic). Simultaneously, the cells were stained with PI.

Assessment of Mitochondrial Changes. The mitochondrial membrane potential was measured with the fluorescent dye JC-1 (Molecular Probes, USA) by flow cytometry, as described previously.[20] The production of ROS was measured by flow cytometry using either HE (Molecular Probes) or H_2DCFDA (Molecular Probes). After different times of treatment, cells were collected by centrifugation and resuspended in HBSS containing the fluorescence probes HE or H_2DCFDA at 2.5 and 0.1 μM, respectively. The cells were incubated for 30 min at 37 °C, centrifuged and resuspended in HBSS. The fluorescence was directly recorded with the flow cytometer, using as excitation wavelength 488 nm and emission at 585 and 530 nm for HE and H_2DCFDA, respectively.

Western Blot Analysis. HeLa cells were incubated in the presence of test compounds and, after different times, were collected, centrifuged, and washed two times with ice cold phosphate-buffered saline (PBS). The pellet was resuspended in lysis buffer. After the cells were lysed on ice for 30 min, lysates were centrifuged at 15000*g* at 4 °C for 10 min. The protein concentration in the supernatant was determined using BCA protein assay reagents (Pierce, Italy). Equal amounts of protein (20 μg) were resolved using sodium dodecyl sulfate–polyacrylamide gel electrophoresis (SDS–PAGE) (7.5–15% acrylamide gels) and transferred to a PVDF Hybond-p membrane (GE Healthcare). Membranes were blocked with I-block (Tropix), the membrane being gently rotated overnight at 4 °C. Membranes were incubated with primary antibodies against Bcl-2, cleaved PARP, cdc25C, Bax, phospho-histone γH2AX and cdc2 (all rabbit, 1:1000, Cell Signaling, Milano, Italy), cyclin B1 (mouse, 1:1000, BD, Milano, Italy), or β-actin (mouse, 1:10,000, Sigma-Aldrich, Milano, Italy) for 2 h at room temperature. Membranes were next incubated with peroxidase-labeled goat antirabbit IgG (1:100,000, Sigma-Aldrich) or peroxidase-labeled goat antimouse IgG (1:100,000, Sigma-Aldrich) for 60 min. All membranes were visualized using ECL Advance (GE Healthcare) and exposed to Hyperfilm MP (GE Healthcare). To ensure equal protein loading, each membrane was stripped and reprobed with anti-β-actin antibody.

Antivascular Activity. HUVECs were prepared from a primary culture of human umbilical cord veins. The adherent cells were maintained in M200 medium supplemented with LSGS (Low Serum Growth Supplement), which contains FBS, hydrocortisone, hEGF, bFGF, heparin, and gentamycin/amphotericin B (Invitrogen, Milano, Italy), and seeded on collagen I (BD Biosciences). Once confluent, the cells were detached by treatment with a trypsin–EDTA solution and used in experiments from the third to seventh passages.

Motility Assay. Motility assay for HUVECs was based on "scratch" wounding of a confluent monolayer.[26] Briefly, HUVECs (1×10^5) were seeded onto 0.3% collagen I-coated six well plates in complete medium until a confluent monolayer was formed. The cells were scratch wounded using a pipet tip. Then the cells were treated with the test compounds, and at different times after the scratch, the cells were photographed under a light microscope (40× magnification). Wound closure was evaluated by Image-J software.

Endothelial Cell Vessel Formation on a Matrigel Matrix. A Matrigel matrix was kept at 4 °C for 16 h. Two hundred microliters of Matrigel (BD Biosciences) was added to each well of a 24-well plate. After gelling at 37 °C for 30 min, gels were overlaid with 500 μL of medium containing 6×10^4 HUVECs. Different concentrations of test compound were added to the cultures, which were incubated for different times. To explore the effect of test compounds on pre-established vasculature, HUVECs were seeded and incubated over Matrigel for 6 h to allow the capillary tubes to form. Then the compound was added and continuously incubated for additional times, and the disappearance of existing vasculature was monitored by recording phase contrast images (five fields for each well: the four quadrants and the center) using a digital camera. The images were saved as TIFF files. Image analysis was carried out using the ImageJ image analysis software and evaluating both dimensional parameters (percent area covered by HUVECs and total length of HUVECs network per field) and topological parameters (number of meshes and branching points per fields).[32] Values were expressed as percent change from control cultures grown with complete medium.

Antitumor Activity *in Vivo*. Four week old female BALB/c-nu nude mice (15–18 g) were obtained from Shanghai SLAC Laboratory Animal Co., Ltd. (Shanghai, China). The animals were maintained under specific pathogen-free conditions with food and water supplied *ad libitum* in Zhejiang University of Traditional Chinese Medicine Laboratory Animal Center. Human colon adenocarcinoma HT-29 cells in logarithmic growth phase were resuspended in RPMI 1640 without fetal bovine serum at 1×10^7cells/mL and inoculated (0.2 mL) in the hypodermis of the pars dorsalis of each mouse. Once the HT-29 xenografts reached a size of ~300 mm^3, 12 mice were randomly assigned to two groups. For the first group, compound **3b** was prepared in DMSO and injected intraperitoneally at volumes of 0.01 mL/g body weight to give a dose of 100 mg/kg to each mouse. The compound was administered three times a week for one week. After completing the treatment schedule and the evaluation period, tumor-bearing mice were euthanized. Tumor volume was calculated by the following formula: $V = (L \times W^2)/2$ where L is the length, and W is the width of the tumor nodules measured by Vernier calipers. The study was approved by the Institutional Animal Ethical Committee of the Second Affiliated Hospital, School of Medicine, Zhejiang University (PRC).

Statistical Analysis. Unless indicated otherwise, results are presented as the mean ± SEM. The differences between different treatments were analyzed using the two-sided Student's t test. P values lower than 0.05 were considered significant.

AUTHOR INFORMATION

Corresponding Author

*(R.R.) Phone: 39-(0)532-455303. Fax: 39-(0)532-455953. E-mail:rmr@unife.it. (P.G.B.) Phone: 39-(0)532-455293. Fax: 39-(0)532-455953. E-mail: pgb@unife.it. (G.V.) Phone: 39-(0)49-8211451. Fax: 39-(0)49-8211462. E-mail:giampietro.viola1@unipd.it.

Notes

The authors declare no competing financial interest.

ACKNOWLEDGMENTS

We thank Dr. Alberto Casolari and Dr. Elisa Durini for excellent technical assistance.

ABBREVIATIONS USED

CA-4, combretastatin A-4; HUVEC, human umbilical vein endothelial cells; EWG, electron-withdrawing group; ERG, electron-releasing group; SAR, structure–activity relationships; CuTc, copper(I)thiophene-2-carboxylate; $Pd_2dba_3{\cdot}CHCl_3$, tris-(dibenzylideneacetone)dipalladium complex with chloroform; TFP, tris(2-furyl)phosphine; FITC, fluorescein isothiocyanate; PI, propidium iodide; PS, phospholipid phosphatidylserine; ROS, reactive oxygen species; HE, hydroxyethidine; H_2DCFDA, 2,7-dichlorodihydrofluorescein; PARP, poly-ADP-ribose polymerase; HBSS, Hank's Balanced Salt Solution; PBS, phosphate-buffered saline; SDS–PAGE, sodium dodecyl sulfate–polyacrylamide gel electrophoresis

REFERENCES

(1) (a) Amos, L. A. Microtubule structure and its stabilisation. *Org. Biomol. Chem.* **2004**, *2*, 2153–2160. (b) Walczak, C. E. Microtubule dynamics and tubulin interacting proteins. *Curr. Opin. Cell. Biol.* **2000**, *12*, 52–56. (c) Risinger, A. L.; Giles, F. J.; Mooberry, S. L. Microtubule dynamics as a target in oncology. *Cancer Treat. Rev.* **2008**, *35*, 255–261.

(2) Downing, K. H.; Nogales, E. Tubulin structure: insights into microtubule properties and functions. *Curr. Opin. Struct. Biol.* **1998**, *8*, 785–791.

(3) (a) Honore, S.; Pasquier, E.; Braguer, D. Understanding microtubule dynamics for improved cancer therapy. *Cell. Mol. Life Sci.* **2005**, *62*, 3039−3056. (b) Pellegrini, F.; Budman, D. R. Review: tubulin function, action of antitubulin drugs, and new drug development. *Cancer Invest.* **2005**, *23*, 264−273 c).

(4) (a) Dumontet, C.; Jordan, M. A. Microtubule-binding agents: a dynamic field of cancer therapeutics. *Nat. Rev. Drug Discovery* **2010**, *9*, 790−803. (b) Screpanti, E.; Santaguida, S.; Nguyen, T.; Silvestri, R.; Guscio, R.; Musacchio, A.; Hamel, E.; De Wulf, P. A screen for kinetochore-microtubule interaction inhibitors identifies novel anti-tubulin compounds. *PLoS One* **2010**, *5*, e11603. (c) Kingston, D. G. Tubulin-Interactive natural products as anticancer agents (1). *J. Nat. Prod.* **2009**, *72*, 507−515.

(5) Pettit, G. R.; Singh, S. B.; Hamel, E.; Lin, C. M.; Alberts, D. S.; Garcia-Kendall, D. Isolation and structure of the strong cell growth and tubulin inhibitor combretastatin A-4. *Experentia* **1989**, *45*, 209−211.

(6) Lin, C. M.; Ho, H. H.; Pettit, G. R.; Hamel, E. Antimitotic natural products combretastatin A-4 and combretastatin A-2: studies on the mechanism of their inhibition of the binding of colchicine to tubulin. *Biochemistry* **1989**, *28*, 6984−6991.

(7) McGown, A. T.; Fox, B. W. Differential cytotoxicity of combretastatins A1 and A4 in two daunorubucin-resistant P388 cell lines. *Cancer Chemother. Pharmacol.* **1990**, *26*, 79−81.

(8) Romagnoli, R.; Baraldi, P. G.; Cara, L. C.; Kimatrai Salvador, M.; Bortolozzi, R.; Basso, G.; Viola, G.; Balzarini, J.; Brancale, A.; Fu, X.-H.; Li, J.; Zhang, S.-Z.; Hamel, E. One-pot synthesis and biological evaluation of 2-pyrrolidinyl-4-amino-5-(3′,4′,5′-trimethoxybenzoyl)-thiazole: a unique, highly active antimicrotubule agent. *Eur. J. Med. Chem.* **2011**, *46*, 6015−6024.

(9) Schwartz, E. L. Antivascular actions of microtubule-binding drugs. *Clin Cancer Res.* **2009**, *15*, 2594−2601.

(10) Tozer, G. M.; Kanthou, C.; Baguley, B. C. Disrupting tumour blood vessels. *Nat. Rev. Cancer* **2005**, *5*, 423−435.

(11) Thomae, D.; Perspicace, E.; Hesse, S.; Kirsch, G.; Seck, P. Synthesis of substituted [1,3]thiazolo[4,5-d][1,2.3]triazines. *Tetrahedron* **2008**, *64*, 9306−9314.

(12) Liebeskind, L. S.; Srogl, J. Heteroaromatic thioether-boronic acid cross-coupling under neutral reaction conditions. *Org. Lett.* **2011**, *3*, 91−93.

(13) Toffoli, G.; Viel, A.; Tuimoto, I.; Bisconti, G.; Rossi, G.; Baoiocchi, M. Pleiotropic-resistant phenotype is a multifactorial phenomenon in human colon carcinoma cell lines. *Br. J. Cancer* **1991**, *63*, 51−56.

(14) Dupuis, M.; Flego, M.; Molinari, A.; Cianfriglia, M. Saquinavir induces stable and functional expression of the multidrug transporter P-glycoprotein in human CD4 T-lymphoblastoid CEM rev cells. *HIV Med.* **2003**, *4*, 338−345.

(15) Martello, L. A.; Verdier-Pinard, P.; Shen, H. J.; He, L.; Torres, K.; Orr, G. A.; Horwitz, S. B. Elevated level of microtubule destabilizing factors in a taxol-resistant/dependent A549 cell line with an alpha-tubulin mutation. *Cancer Res.* **2003**, *63*, 448−454.

(16) (a) Hamel, E. Evaluation of antimitotic agents by quantitative comparisons of their effects on the polymerization of purified tubulin. *Cell Biochem. Biophys.* **2003**, *38*, 1−21. (b) Verdier-Pinard, P.; Lai, J.-Y.; Yoo, H.-D.; Yu, J.; Marquez, B.; Nagle, D. G.; Nambu, M.; White, J. D.; Falck, J. R.; Gerwick, W. H.; Day, B. W.; Hamel, E. Structure-activity analysis of the interaction of curacin A, the potent colchicine site antimitotic agent, with tubulin and effects of analogs on the growth of MCF-7 breast cancer cells. *Mol. Pharmacol.* **1998**, *53*, 62−67. (c) Hiser, L.; Aggarwal, A.; Young, R.; Frankfurter, A.; Spano, A.; Correia, J. J.; Lobert, S. Comparison of β-tubulin mRNA and protein levels in 12 human cancer cell lines. *Cell Motil. Cytoskeleton* **2006**, *63*, 41−52.

(17) Massarotti, A.; Coluccia, A.; Silvestri, R.; Sorba, G.; Brancale, A. The tubulin colchicine domain: a molecular modeling perspective. *ChemMedChem* **2012**, *7*, 33−42.

(18) (a) Mollinedo, F.; Gajate, C. Microtubules, microtubule-interfering agents and apoptosis. *Apoptosis* **2003**, *8*, 413−450. (b) Clarke, P. R.; Allan, L. A. Cell-cycle control in the face of damage- a matter of life or death. *Trends Cell Biol.* **2009**, *19*, 89−98.

(19) (a) Ly, J. D.; Grubb, D. R.; Lawen, A. The mitochondrial membrane potential ($\Delta\psi_m$) in apoptosis: an update. *Apoptosis* **2003**, *3*, 115−128. (b) Green, D. R.; Kroemer, G. The pathophysiology of mitochondrial cell death. *Science* **2005**, *305*, 626−629.

(20) Viola, G.; Fortunato, E.; Cecconet, L.; Del Giudice, L.; Dall'Acqua, F.; Basso, G. Central role of mitochondria and p53 in PUVA-induced apoptosis in human keratinocytes cell line NCTC-2544. *Toxicol. Appl. Pharmacol.* **2008**, *227*, 84−96.

(21) (a) Cai, J.; Jones, D. P. Superoxide in apoptosis. Mitochondrial generation triggered by cytochrome *c* loss. *J. Biol. Chem.* **1998**, *273*, 11401−11404. (c) Nohl, H.; Gille, L.; Staniek, K. Intracellular generation of reactive oxygen species by mitochondria. *Biochem. Pharmacol.* **2005**, *69*, 719−723.

(22) Rothe, G.; Valet, G. Flow cytometric analysis of respiratory burst activity in phagocytes with hydroethidine and 2′,7′-dichloro-fluorescein. *J. Leukocyte Biol.* **1990**, *47*, 440−448.

(23) (a) Porter, A. G.; Janicke, R. U. Emerging role of caspase-3 in apoptosis. *Cell Death Differ.* **1999**, *6*, 99−104. (b) Kumar, S. Caspase function in programmed cell death. *Cell Death Differ.* **2007**, *14*, 32−43.

(24) Kuo, L. J.; Yang, L. X. Gamma-H2AX - a novel biomarker for DNA double-strand breaks. *In Vivo* **2008**, *22*, 305−309.

(25) Matson, D. R.; Stukenberg, P. T. Spindle poisons and cell fate: a tale of two pathways. *Mol. Interventions* **2011**, *11*, 141−50.

(26) Vincent, L.; Kermani, P.; Young, L. M.; Cheng, J.; Zhang, F; Shido, K; Lam, G.; Bompais-Vincent, H.; Zhu, Z.; Hicklin, D. J.; Bohlen, P.; Chaplin, D. J.; May, C.; Rafii, S. Combretastatin A4 phosphate induces rapid regression of tumor neovessels and growth through interference with vascular endothelial-cadherin signaling. *J. Clin. Invest.* **2005**, *115*, 2992−3006.

(27) Dalyot-Herman, N.; Delgado-Lopez, F.; Gewirtz, D. A.; Gupton, J. T.; Schwartz, E. L. Interference with endothelial cell function by JG-03−14, an agent that binds to the colchicine site on microtubules. *Biochem. Pharmacol.* **2009**, *78*, 1167−77J.

(28) Liang, C. C.; Park, A. Y.; Guan, J. L. In vitro scratch assay: a convenient and inexpensive method for analysis of cell migration in vitro. *Nat. Protoc.* **2007**, *2*, 329−33.

(29) Dorleans, A.; Gigant, B.; Ravelli, R. B.; Mailliet, P.; Mikol, V.; Knossow, M. Variations in the colchicine-binding domain provide insight into the structural switch of tubulin. *Proc. Natl. Acad. Sci. U.S.A.* **2009**, *106*, 13775−13779.

(30) *Molecular Operating Environment (MOE 2010)*; Chemical Computing Group, Inc.: Montreal, Quebec, Canada. http://www.chemcomp.com.

(31) Korb, O.; Stützle, T.; Exner, T. E. PLANTS: Application of Ant Colony Optimization to Structure-Based Drug Design. In *Ant Colony Optimization and Swarm Intelligence*, 5th International Workshop, ANTS 2006, Brussels, Belgium, Sep 4−7, 2006; Dorigo, M., Gambardella, L. M., Birattari, M., Martinoli, A., Poli, R., Sttzle, T., Eds.; Springer: Berlin, 2006; LNCS 4150, pp 247−258.

(32) Guidolin, D.; Vacca, A.; Nussdorfer, G. G.; Ribatti, D. A. New image analysis method based on topological and fractal parameters to evaluate the angiostatic activity of docetaxel by using the Matrigel assay in vitro. *Microvasc. Res.* **2004**, *67*, 117−24.